

Sub-unity superfluid fraction of a supersolid from self-induced Josephson effect

Giulio Biagioni,^{1,2,*} Nicolò Antolini,^{2,3,*} Beatrice Donelli,^{3,4,5,6} Luca Pezzè,^{3,4,5} Augusto Smerzi,^{3,4,5,†} Marco Fattori,^{1,3,7} Andrea Fioretti,² Carlo Gabbanini,² Massimo Inguscio,^{3,8} Luca Tanzi,^{2,3} and Giovanni Modugno^{1,2,3,‡}

¹*Dipartimento di Fisica e Astronomia, Università degli studi di Firenze,*

Via G. Sansone 1, 50019 Sesto Fiorentino, Italy

²*CNR-INO, sede di Pisa, Via Moruzzi 1, 56124 Pisa, Italy*

³*European Laboratory for Nonlinear Spectroscopy,*

Università degli studi di Firenze, Via N. Carrara 1, 50019 Sesto Fiorentino, Italy

⁴*CNR-INO, sede di Firenze, Largo Enrico Fermi 5, 50125 Firenze, Italy*

⁵*QSTAR, Largo Enrico Fermi 2, 50125 Firenze, Italy*

⁶*Università degli studi di Napoli “Federico II”, Via Cinthia 21, 80126 Napoli, Italy*

⁷*CNR-INO, sede di Sesto Fiorentino, Via N. Carrara 1, 50019 Sesto Fiorentino, Italy*

⁸*Dipartimento di Ingegneria, Università Campus Bio-Medico di Roma, Via Alvaro Del Portillo 21, 00128 Roma, Italy*

(Dated: November 9, 2023)

Recently, a novel class of superfluids and superconductors with spontaneous spatially-periodic modulation of the superfluid density has been discovered in a variety of systems [1–12]. They might all be related to the concept of a supersolid phase of matter, which has by definition a macroscopic wavefunction with spatial modulation originating from the simultaneous, spontaneous breaking of the gauge and translational symmetries [13–16]. However, this relation has only been recognized in some cases [1, 2, 5–9] and there is the need for universal properties quantifying the differences between supersolids and ordinary superfluids/superconductors or ordinary crystals. A key property is the superfluid fraction [16], which measures the reduction in superfluid stiffness due to the spatial modulation, leading to the non-standard superfluid dynamics of supersolids [16–18]. The superfluid fraction was introduced long ago, but until now its predicted sub-unity value has not been quantitatively assessed in any supersolid candidate. Here we propose and demonstrate an innovative method to measure the superfluid fraction of a supersolid based on the Josephson effect, a phenomenon ubiquitous in superfluids and superconductors, associated with the presence of a physical barrier between two superfluids [19]. We show that in a supersolid the Josephson effect arises spontaneously, without the need of a barrier, due to the spontaneous spatial modulation. Individual lattice cells of the supersolid lattice behave as self-induced Josephson junctions, and from the dynamics of the Josephson oscillations we can derive directly the local superfluid fraction. Our investigation is carried out on a cold-atom dipolar supersolid [7], for which we discover a relatively large sub-unity superfluid fraction that makes realistic the study of novel phenomena such as partially quantized vortices and supercurrents [16–18]. Our methods and results are very general and open a new direction of research that may unify the description of all supersolid-like systems. Our work also discloses a new type of Josephson junction.

Supersolids are a fundamental phase of matter originated by the spontaneous breaking of the gauge symmetry as in superfluids and superconductors, and of the translational symmetry as in crystals [13–16]. This gives rise to a macroscopic wavefunction with spatially-periodic modulation, and to mixed superfluid and crystalline properties. Supersolids were originally predicted in the context of solid helium [13–16]. Today, quantum phases with spontaneous modulation of the wavefunction are under study in a variety of bosonic and fermionic systems. These include: the second layer of ⁴He on graphite [1, 2]; ultracold quantum gases in optical cavities [5], with spin-orbit coupling [6], or with strong dipolar interactions [7–9, 20]; the pair density wave phase of ³He under confinement [3, 4]; pair density wave phases in various types of superconductors

[10–12]. Related phases have been proposed to exist in the crust of neutron stars [21] and for excitons in semiconductor heterostructures [22]. All these systems might be connected to supersolidity, which however so far has emerged clearly only in some cold-atom systems with the evidence of the double spontaneous breaking and of the mixed superfluid-crystalline character [5, 23, 24]. The experiments carried out so far on the other types of systems have proved the coexistence of superfluidity/superconductivity and crystal-like structure [1–4, 10–12], but no quantitative connection of the observations to the concept of supersolidity has been made. One of the difficulties in comparing different types of systems with spatial modulation of the wavefunction is the seeming lack of a universal property quantifying the deviations from the dynamical behavior of ordinary superfluids or superconductors.

* These authors contribute equally

† augusto.smerzi@ino.cnr.it

‡ modugno@lens.unifi.it

Here we note that a property with such characteristics already exists, the so-called superfluid fraction of supersolids, well known in the field of superfluids but not

in the one of superconductors. The superfluid fraction, introduced by A. J. Leggett in 1970 [16], quantifies the effect of the spatial modulation on the superfluid stiffness, which is in itself a defining property of superfluids and superconductors. The superfluid stiffness indeed measures the finite energy cost of twisting the phase of the macroscopic wavefunction and accounts for all fundamental phenomena of superfluidity, such as phase coherence, quantized vortices and supercurrents [25]. As shown in Fig. 1, while in a homogeneous superfluid/superconductor the phase varies linearly in space, in a modulated system most of the phase variation can be accommodated in the minima of the density, reducing the energy cost. Since the superfluid velocity is the gradient of the phase, this implies that peaks and valleys should move differently, giving rise to complex dynamics with mixed classical (crystalline) and quantum (superfluid) character. For example, fundamental superfluid phenomena like vortices and supercurrents are predicted to be profoundly affected by the presence of the spatial modulation, losing the canonical quantization of their angular momentum [16–18, 26]. The superfluid fraction, which ranges from unity for standard superfluids to zero for standard crystals, enters directly in all these phenomena and is therefore the proper quantity to assess the deviations from standard superfluids and superconductors. Note that the superfluid fraction of supersolids is not related to thermal effects, in contrast to the superfluid fraction due to the thermal depletion of superfluids and superconductors [27].

The standard methods to measure the superfluid stiffness are based on the measurement of global properties such as the moment of inertia for rotating superfluids [1, 4], or the penetration depth of the magnetic field for superconductors [28]. In dipolar supersolids, previous attempts using rotational techniques revealed a large superfluid fraction [29], but were not precise enough to assess its sub-unity value [30, 31]. In the other systems there is evidence that the superfluid stiffness is low [1, 2, 28], but no quantitative measurement of a sub-unity superfluid fraction is available.

In this work we make a paradigm shift, demonstrating that it is possible to measure the superfluid fraction not only from global dynamics but also from a fundamental phenomenon taking place in individual cells of a supersolid: the Josephson effect [19]. In Fig. 1, one can note a similarity between individual cells of the supersolid and Josephson junctions, having the same structure of two bulk superfluids connected by a weak link. It is therefore tempting to associate supersolidity to the very existence of local Josephson dynamics. However, so far the Josephson effect in supersolids has not been studied beyond the phenomenological modelling of the relaxation towards the ground state in a cold-atom system [32]. There is no theoretical or experimental evidence for local Josephson oscillations, nor an understanding of the

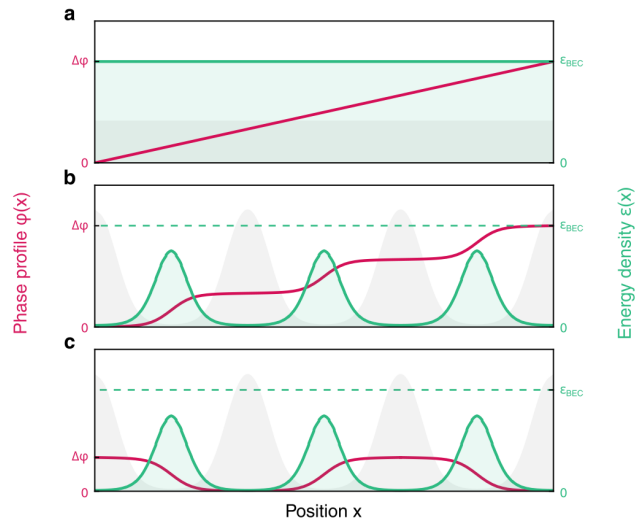


FIG. 1. Sketch of the superfluid fraction from the application of a phase twist in a bosonic system at zero temperature. (a) In a homogeneous superfluid a phase twist with amplitude $\Delta\varphi$ results in a constant gradient of the phase, i.e. a constant velocity, while in a supersolid (b,c) the kinetic energy can be minimised by accumulating most of the phase variation in the low-density regions. The grey and green areas represent the number density and the kinetic energy density respectively, while the phase profile is plotted in red. The superfluid fraction is the ratio of the area under the green curve to that of the homogeneous case. (b) Leggett’s approach, which for an annular system would correspond to a stationary rotation, leads to a monotonous increase of the phase. (c) Our method, based on an alternating oscillation of the phase, leads to Josephson oscillations. Both kinetic energy and superfluid fraction are the same for (b) and (c).

potential relation between the Josephson effect and the superfluid stiffness. The problem is complicated by the fact that, in supersolids, the weak links are self-induced by internal interactions rather than by an external potential, so they can change during the dynamics. Therefore it is not clear if phenomena such as Josephson oscillations can exist at all in a supersolid.

Here we demonstrate that a supersolid can in fact sustain coherent phase-density oscillations, behaving as an array of Josephson junctions. We also show that the Josephson coupling energy that one can deduce from the Josephson oscillations provides a direct measurement of the local superfluid fraction. We use this novel approach to measure with high precision the superfluid fraction of the dipolar supersolid appearing in a quantum gas of magnetic atoms. We find a whole range of sub-unity values of the superfluid fraction, depending on the depth of the density modulation in accordance with Leggett’s predictions.

Leggett’s approach to the superfluid fraction considers an annular supersolid in the rotating frame and maps it

to a linear system with an overall phase twist, as sketched in Fig. 1b. The superfluid fraction is defined on a unit cell as [16, 33]

$$f_s = \frac{E_{kin}}{E_{kin}^{hom}}. \quad (1)$$

The numerator is the kinetic energy acquired by the supersolid with number density $n(x)$ when applying a phase $\Delta\varphi$ twist over a lattice cell of length d , $E_{kin} = \hbar^2/(2m) \int_{\text{cell}} dx n(x) |\nabla\varphi(x)|^2$, and thus accounts for density and phase modulations. The denominator $E_{kin}^{hom} = Nmv_s^2/2$ is the kinetic energy of a homogeneous superfluid of N atoms and velocity $v_s = \hbar\Delta\varphi/(md)$ associated with a constant phase gradient across the cell. Using a variational approach [16, 34], Leggett found an upper and a lower bound for Eq. 1, $f_s^l \leq f_s \leq f_s^u$, see Methods. In particular, the upper bound

$$f_s^u = \left(\frac{1}{d} \int_0^d \frac{dx}{\bar{n}(x)} \right)^{-1} \quad (2)$$

where $\bar{n}(x)$ is the normalised 1D density, restricts f_s to be lower than unity if the density is spatially modulated.

We propose an alternative expression for the superfluid fraction, considering Josephson phase twists with alternating sign between neighbouring lattice sites of a supersolid, as sketched in Fig. 1c. This corresponds to a different type of motion of the supersolid, with no global flow but with alternate Josephson phase-density oscillations between sites. Also in this case we can consider a single cell, since the kinetic energy is proportional to $|\nabla\varphi(x)|^2$, so it does not depend on the sign of the phase twist. In the limit of small excitations ($\Delta\varphi \rightarrow 0$), the kinetic energy of a Josephson junction is given by $E_{kin} = NK|\nabla\varphi|^2$, where K is the coupling energy across the barrier [35]. From Eq. 1 we thus find:

$$f_s = \frac{K}{\hbar^2/(2md)^2} \quad (3)$$

showing a direct relation between the superfluid fraction and the coupling energy of the junction. We note that an expression similar to the upper bound in Eq. 2 was derived by Leggett for the coupling energy of a single Josephson junction [36], however without discussing the connection to the superfluid fraction.

We now demonstrate the existence of coherent Josephson-like oscillations in a dipolar supersolid [7]. This system is particularly appealing to study fundamental aspects of supersolidity: the supersolid lattice is macroscopic, with many atoms per site and large superfluid effects; the available control of the quantum phase

transition allows to directly compare supersolids and superfluids; interactions are weak, allowing accurate theoretical modelling. Our experimental system is composed of about $N = 3 \times 10^4$ bosonic dysprosium atoms, held in a harmonic trap elongated along the x direction, with trap frequencies $(\omega_x, \omega_y, \omega_z) = 2\pi \times (18, 97, 102)$ Hz. By tuning the relative strength ϵ_{dd} of dipolar and contact interactions, we can cross the quantum phase transition from a standard Bose-Einstein condensate to the supersolid regime (Methods). The supersolid lattice structure is one-dimensional, leading to a continuous phase transition [37]. Our typical supersolid is made of two main central clusters and four smaller lateral ones, with a lattice period $d \sim 4 \mu\text{m}$, as shown in Fig. 2. We can vary the density modulation depth by varying the interaction strength in the range $\epsilon_{dd} = 1.38 - 1.45$; further increasing ϵ_{dd} leads to the formation of an incoherent crystal of separate clusters, the so-called droplet crystal, a regime that we cannot study experimentally due to its short lifetime [7].

We find that the application for a short time of an optical lattice with twice the spacing of the supersolid (sketched in Fig. 2a) imprints the proper alternating phase difference between adjacent clusters to excite Josephson oscillations. With a depth of 100 nK and an application time of $\tau = 100 \mu\text{s}$ we obtain a phase difference of the order of $\pi/2$. After a variable evolution time in the absence of the lattice, we measure both the evolving phase difference $\Delta\varphi$ between neighboring clusters and the population imbalance Z between the left and right halves of the supersolid. $\Delta\varphi$ is measured from the interference fringes developing after a free expansion (snapshots in Fig. 2b, top row), while Z is measured by in-situ phase-contrast imaging (Fig. 2b, bottom row) (Methods). As shown in Fig. 2c-d, we observe single-frequency oscillations of Z and $\Delta\varphi$, with the characteristic $\pi/2$ phase shift of the standard Josephson dynamics [19, 35, 38–41]. The observation time is limited to about 100 ms by the finite lifetime of the supersolid, due to unavoidable particle losses [7]. The experimental observations agree very well with numerical simulations based on the time-dependent extended Gross-Pitaevskii equation, also shown in Fig. 2c-d (Methods). We have checked that the Josephson oscillations are not observable if we apply the same procedure to standard Bose-Einstein condensates, instead of supersolids (see Methods).

The observation of a single frequency in both experiment and simulations indicates not only that it is possible to excite Josephson-like oscillations in a supersolid, but also that they are a normal mode of the system. To model our observations, we develop a six-mode model, generalising the two-mode Josephson oscillations [35] to the case of six clusters (see Methods). We associate to the j th cluster a population N_j and a phase φ_j ($j = 1, \dots, 6$). In general, the dynamics include contributions from each cluster and show multiple frequencies. However, we find

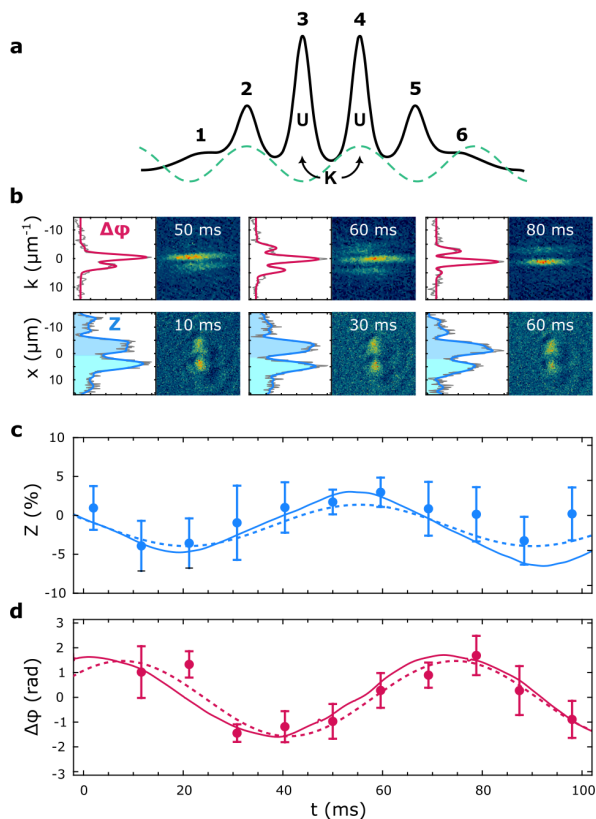


FIG. 2. Josephson oscillations in a supersolid. (a) Sketch of the experimental system. The black line is the supersolid density profile at equilibrium. The green dashed line is the optical lattice potential used for the phase imprinting. (b) Examples of experimental single shots and corresponding integrated 1D profiles. Top row: interference fringes after a free expansion. Red curves are fit functions used to extract the phase difference $\Delta\varphi$. Bottom row: in-situ images. Shaded areas indicate the populations of the left and right halves of the supersolid used to extract the population imbalance Z . (c) Oscillations of Z as a function of time at $\epsilon_{dd} = 1.428$. Dots are experimental points. The solid line is the numerical simulation for the same parameters. The dotted line is a sinusoidal fit to the experimental data. (d) Same for $\Delta\varphi$.

that, under appropriate conditions among the interaction and coupling energies, there exists a normal mode of the system where the dynamical variables of the two central clusters of the supersolid decouple from the lateral ones. This results in Josephson-like oscillations described by the two coupled equations

$$\Delta\dot{N} = -4KN_{34}\sin\Delta\varphi, \quad (4a)$$

$$\Delta\dot{\varphi} = U\Delta N, \quad (4b)$$

where $\Delta N = N_3 - N_4$, $N_{34} = N_3(0) + N_4(0)$ and $\Delta\varphi = \varphi_3 - \varphi_4$. These equations hold for interaction energies $N_{34}U$ much larger than K (for our system, $N_{34}U/(2K) > 25$, see Methods). Since in our case

$\Delta N \ll N$, we keep only linear terms in $\Delta N/N$.

Equations 4 are equivalent to those of a simple pendulum with angle $\Delta\varphi$ and angular momentum ΔN , and in the small-angle limit feature sinusoidal oscillations with a single frequency, $\omega_J = \sqrt{4KN_{34}}$. We emphasise that the current-phase relation Eq. 4a as well as ω_J^2 differ by a factor 2 with respect to the Josephson equations of two weakly coupled Bose-Einstein condensates, due to the contribution of the lateral clusters. Notice also that Eqs. 4 depend only on the coupling energy K and the interaction energy U of the two central clusters, in contrast to the expectation that the inhomogeneity of the trapped system may introduce other energies in the equations of motion. We checked by Gross-Pitaevskii simulations that our experimental configuration satisfies the conditions to have a Josephson-like normal mode (namely Eq. S6 of the Methods).

In the experiment we are not able to resolve the population of the individual clusters, but we study the population difference between the left and right halves of the system, $Z = (N_1 + N_2 + N_3 - N_4 - N_5 - N_6)/N$. There is a proportionality relation between the two observables, $\Delta N = 2NZ$, which allows us to rewrite Eqs. 4 in terms of the experimental observables (Methods).

An important difference between a cell of the supersolid and a standard Josephson junction is the fact that in the supersolid the position of the weak link is not fixed by an external barrier but it is self-induced, so it can move. This leads to the appearance of a low-energy Goldstone mode associated with the spontaneous translational symmetry breaking. In a harmonic potential, it consists of a slow oscillation of the position of the weak link, together with the density maxima, and an associated oscillation of both Z and $\Delta\varphi$ [24]. Due to its low frequency (few Hz), the Goldstone mode is spontaneously excited by thermal fluctuations, resulting in shot-to-shot fluctuations of the experimental observables. The same low frequency, however, allows to separate Josephson and Goldstone dynamics in both experiment and theory (Methods).

We measure the Josephson frequency ω_J from a sinusoidal fit of the phase and population dynamics in Fig. 2c-d. We repeat the measurement by varying the interaction parameter ϵ_{dd} , corresponding to different depths of the supersolid density modulation. Figure 3 shows the fitted frequencies as a function of ϵ_{dd} and a comparison with the numerical simulations. We observe a decrease of the frequency for increasing ϵ_{dd} . This is justified by the fact that the superfluid current across the junction decreases because a larger and larger portion of the wavefunction remains localised inside the clusters, see insets in Fig. 3. This reduces the coupling energy K while only weakly affecting the interaction energy. From the Josephson frequency we can derive the coupling

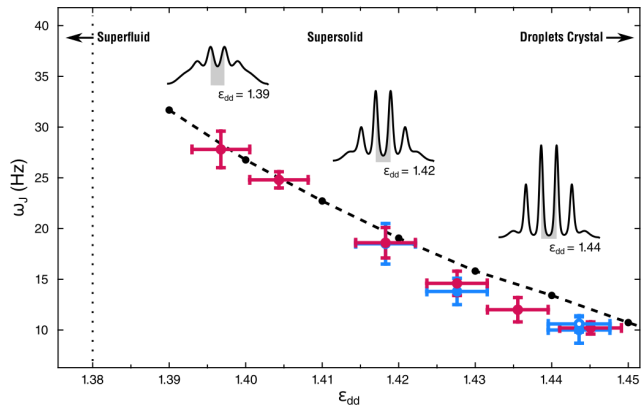


FIG. 3. Josephson oscillation frequencies as a function of the interaction parameter ϵ_{dd} . Red dots are the experimental frequencies for $\Delta\varphi$. Filled and open blue dots are the frequencies for Z measured by in situ imaging with and without optical separation, respectively (Methods). The red point at $\epsilon_{dd} = 1.444$ is slightly shifted horizontally for clarity. Black points are the results of numerical simulations. The dashed line is a guide for the eye. The insets show the modulated ground state density profiles obtained from numerical simulations for different values of ϵ_{dd} . The vertical dotted line marks the critical point of the superfluid-supersolid quantum phase transition.

energy as $K = \omega_J^2/(4UN_{34})$, with the denominator obtained from the simulations. We verified that this relation holds not only in the small-amplitude regime of the simulations, but also for the larger amplitudes of the experiment.

From the measured K , we derive in turn the superfluid fraction using Eq. 3. The results are shown in Figure 4 and feature a progressive reduction of the superfluid fraction below unity for increasing depths of the supersolid modulation. The experimental data are in good agreement with the numerical simulations (green dots), where according to Eq. 4a the coupling energy is obtained from the linear dependence of dZ/dt on $\sin(\Delta\varphi)$ (current-phase relation), see Fig. 4b. A similar analysis (Fig. 4c) was performed on the experimental data for which we have combined phase and population oscillations (pink dots in Fig. 4a). The results for these data points demonstrate the reduced superfluid fraction of the supersolid with no numerical input on the interaction energy U .

What we measure here is the superfluid fraction of the central cell of our inhomogeneous supersolid, for a one-dimensional phase twist. Such a local quantity would coincide with the global superfluid fraction of a hypothetical homogeneous supersolid, composed of cells identical to our central one. This includes the annular geometry originally studied by Leggett, where however our supersolid with macroscopic clusters would also

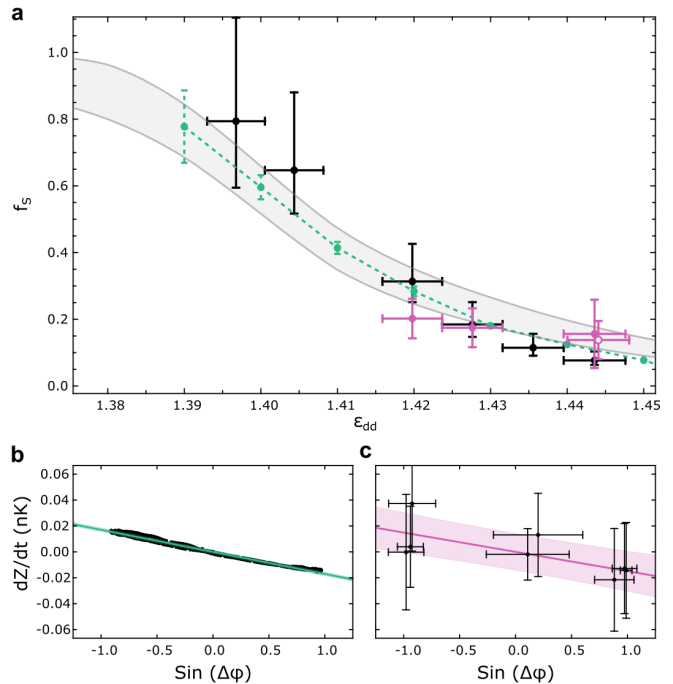


FIG. 4. Superfluid fraction of the supersolid from Josephson oscillations. (a) Superfluid fraction as a function of ϵ_{dd} . Black dots are experimental results derived from the Josephson frequencies. Green dots are results from numerical simulations. Pink points are derived from the experimental phase-current relation, as in (c). The open pink point at $\epsilon_{dd} = 1.444$ is the dataset without the optical separation technique (see Methods). The grey band spans from the upper to the lower bound of Eq. 2. (b-c) Phase-current relation at $\epsilon_{dd} = 1.444$. The points show the results of numerical simulations (b) and experimental measurements (c), respectively. From the linear regressions (green and pink lines) we extract the coupling energy K according to Eq. 4a. The shaded regions are the confidence bands for one standard deviation.

show transverse effects, not included in Leggett's theory for the moment of inertia [16]. Studying the Josephson effect allows us to avoid such transverse effects.

In Fig. 4a we also compare our results with Leggett's prediction of Eq. 2, relating the superfluid fraction to the density modulation of the supersolid. From the numerical density profiles, we calculate both the upper bound f_s^u and the corresponding lower bound [34] f_s^l , which delimit the grey area in Fig. 4a (see Methods). The two bounds would coincide if the density distribution were separable in the transverse coordinates y and z . Since our supersolid lattice is one-dimensional, the two bounds are close to each other. The superfluid fraction calculated from the simulated dynamics lies between the two bounds in the whole supersolid region we investigated, demonstrating the applicability of Leggett's result to our system.

In conclusion, the overall agreement between experi-

ment, simulations and theory on our dipolar supersolid proves the long-sought sub-unity superfluid fraction of supersolids and its relation to the spatial modulation of the superfluid density. The demonstration of self-sustained Josephson oscillations in a supersolid not only establishes an analogy between supersolids and Josephson junction arrays, but also provides a novel proof of the extraordinary nature of supersolids compared to ordinary superfluids and crystals. These oscillations indeed cannot exist neither in crystals, where particles are bound to lattice sites, nor in ordinary superfluids, which do not have a lattice structure.

Our findings open new research directions. The observed reduction of the superfluid fraction with increasing modulation depths may explain the low superfluid stiffness measured in other systems, such as ^4He on graphite [1, 4] or superconductors hosting pair-density-wave phases [10–12]. An important question related to the pair density waves in fermionic systems is how Leggett’s bounds on the superfluid fraction may be extended to systems where the superfluid density and particle density do not coincide. Note that Eq. 2 is also applicable to standard superfluids with an externally-imposed spatial modulation, as demonstrated for Bose-Einstein condensates in optical lattices via measurements of the effective mass [38] or of the sound velocity [42, 43]. In the supersolid, however, the dynamics linked to the reduced superfluid fraction is not constrained by an external potential, and so totally new phenomena might be observed. The large value of f_s we measured for the dipolar supersolid, which remains larger than 10% also for deep density modulations, indicates that partially quantized supercurrents [16, 18] and vortices [17] should appear at a macroscopic level.

Due to the generality of the Josephson effect, our Josephson-oscillation technique might be applied to characterise the local superfluid dynamics of the other supersolid-like phases under study in superfluid and

superconducting systems. Eq. 3 is applicable in general, considering that the detection of Josephson oscillations implies measurement of both the coupling energy and the spatial period of the superfluid density modulation. For example, a promising type of system may be the pair-density wave phase in superconductors, where the modulation has already been resolved.

Additionally, the self-induced Josephson junctions we have identified in supersolids might have extraordinary properties due to the mobility of the weak links. Indeed, although the Goldstone mode of the weak links is not relevant for the Josephson dynamics due to its very low energy, for the same reason it may affect the fluctuation properties of the junction [44], potentially leading to new thermometry methods [45], and especially to novel entanglement properties [46].

ACKNOWLEDGMENTS

Funded by the European Union (ERC, SUPERSOLIDS, n. 101055319), by the QuantERA Programme that has received funding from the European Union’s Horizon 2020 research and innovation programme under Grant Agreements 731473 and 101017733, projects MENTA and MAQS, with funding organisation Consiglio Nazionale delle Ricerche. Technical assistance from A. Barbini, A. Hajeb, F. Pardini, M. Tagliaferri and M. Voliani is gratefully acknowledged.

CONTRIBUTIONS

N. A., G. B., A. F., C. G., L. T. and G. M. performed the experimental measurements. B. D., L. P., and A. S. developed the theoretical model and carried out the numerical simulations. N. A., G. B., B. D., and L. P. performed the experiment-theory comparison. N. A., G. B., B. D., L. P., A. S., A. F., M. F., C. G., M. I., L. T. and G. M contributed to the interpretation of the results and the writing of the paper.

-
- [1] J. Nyéki, A. Phillis, A. Ho, D. Lee, P. Coleman, J. Parpia, B. Cowan, and J. Saunders, Intertwined superfluid and density wave order in two-dimensional ^4He , *Nature Physics* **13**, 455 (2017).
 - [2] J. Choi, A. A. Zadorozhko, J. Choi, and E. Kim, Spatially modulated superfluid state in two-dimensional ^4He films, *Phys. Rev. Lett.* **127**, 135301 (2021).
 - [3] L. V. Levitin, B. Yager, L. Sumner, B. Cowan, A. J. Casey, J. Saunders, N. Zhelev, R. G. Bennett, and J. M. Parpia, Evidence for a spatially modulated superfluid phase of ^3He under confinement, *Phys. Rev. Lett.* **122**, 085301 (2019).
 - [4] A. J. Shook, V. Vadakkumbatt, P. Senarath Yapa, C. Doolin, R. Boyack, P. H. Kim, G. G. Popowich, F. Souris, H. Christani, J. Maciejko, and J. P. Davis, Stabilized pair density wave via nanoscale confinement of superfluid ^3He , *Phys. Rev. Lett.* **124**, 015301 (2020).
 - [5] J. Léonard, A. Morales, P. Zupancic, T. Esslinger, and T. Donner, Supersolid formation in a quantum gas breaking a continuous translational symmetry, *Nature* **543**, 87 (2017).
 - [6] J.-R. Li, J. Lee, W. Huang, S. Burchesky, B. Shteynas, F. Ç. Top, A. O. Jamison, and W. Ketterle, A stripe phase with supersolid properties in spin-orbit-coupled bose-einstein condensates, *Nature* **543**, 91 (2017).
 - [7] L. Tanzi, E. Lucioni, F. Famà, J. Catani, A. Fioretti, C. Gabbanini, R. N. Bisset, L. Santos, and G. Modugno, Observation of a dipolar quantum gas with metastable

- supersolid properties, *Phys. Rev. Lett.* **122**, 130405 (2019).
- [8] F. Böttcher, J.-N. Schmidt, M. Wenzel, J. Hertkorn, M. Guo, T. Langen, and T. Pfau, Transient supersolid properties in an array of dipolar quantum droplets, *Phys. Rev. X* **9**, 011051 (2019).
- [9] L. Chomaz, D. Petter, P. Ilzhöfer, G. Natale, A. Trautmann, C. Politi, G. Durastante, R. M. W. van Bijnen, A. Patscheider, M. Sohmen, M. J. Mark, and F. Ferlaino, Long-lived and transient supersolid behaviors in dipolar quantum gases, *Phys. Rev. X* **9**, 021012 (2019).
- [10] M. H. Hamidian, S. D. Edkins, S. H. Joo, A. Kostin, H. Eisaki, S. Uchida, M. J. Lawler, E.-A. Kim, A. P. Mackenzie, K. Fujita, J. Lee, and J. C. S. Davis, Detection of a cooper-pair density wave in $\text{Bi}_2\text{Sr}_2\text{CaCu}_2\text{O}_{8+x}$, *Nature* **532**, 343 (2016).
- [11] Y. Liu, T. Wei, G. He, Y. Zhang, Z. Wang, and J. Wang, Pair density wave state in a monolayer high- T_c iron-based superconductor, *Nature* **618**, 934 (2023).
- [12] D. F. Agterberg, J. S. Davis, S. D. Edkins, E. Fradkin, D. J. Van Harlingen, S. A. Kivelson, P. A. Lee, L. Radzihovsky, J. M. Tranquada, and Y. Wang, The physics of pair-density waves: Cuprate superconductors and beyond, *Annual Review of Condensed Matter Physics* **11**, 231 (2020), <https://doi.org/10.1146/annurev-conmatphys-031119-050711>.
- [13] E. P. Gross, Unified theory of interacting bosons, *Phys. Rev.* **106**, 161 (1957).
- [14] A. F. Andreev and I. M. Lifshitz, Quantum theory of defects in crystals, *Soviet Physics Uspekhi* **13**, 670 (1971).
- [15] G. V. Chester, Speculations on Bose-Einstein Condensation and Quantum Crystals, *Phys. Rev. A* **2**, 256 (1970).
- [16] A. J. Leggett, Can a solid be “superfluid”?, *Phys. Rev. Lett.* **25**, 1543 (1970).
- [17] A. Gallemí, S. M. Rocuzzo, S. Stringari, and A. Recati, Quantized vortices in dipolar supersolid bose-einstein-condensed gases, *Phys. Rev. A* **102**, 023322 (2020).
- [18] M. N. Tengstrand, D. Bohlm, R. Sachdeva, J. Bengtsson, and S. M. Reimann, Persistent currents in toroidal dipolar supersolids, *Phys. Rev. A* **103**, 013313 (2021).
- [19] B. Josephson, Possible new effects in superconductive tunnelling, *Physics Letters* **1**, 251 (1962).
- [20] M. A. Norcia, C. Politi, L. Klaus, E. Poli, M. Sohmen, M. J. Mark, R. N. Bisset, L. Santos, and F. Ferlaino, Two-dimensional supersolidity in a dipolar quantum gas, *Nature* **596**, 357 (2021).
- [21] C. J. Pethick, N. Chamel, and S. Reddy, Superfluid Dynamics in Neutron Star Crusts, *Progress of Theoretical Physics Supplement* **186**, 9 (2010), <https://academic.oup.com/ptps/article-pdf/doi/10.1143/PTPS.186.9/28674848/186-9.pdf>.
- [22] S. Conti, A. Perali, A. R. Hamilton, M. V. Milošević, F. m. c. M. Peeters, and D. Neilson, Chester supersolid of spatially indirect excitons in double-layer semiconductor heterostructures, *Phys. Rev. Lett.* **130**, 057001 (2023).
- [23] L. Tanzi, S. M. Rocuzzo, E. Lucioni, F. Famà, A. Fioretti, C. Gabbanini, G. Modugno, A. Recati, and S. Stringari, Supersolid symmetry breaking from compressional oscillations in a dipolar quantum gas, *Nature* **574**, 382 (2019).
- [24] M. Guo, F. Böttcher, J. Hertkorn, J.-N. Schmidt, M. Wenzel, H. P. Büchler, T. Langen, and T. Pfau, The low-energy goldstone mode in a trapped dipolar supersolid, *Nature* **574**, 386 (2019).
- [25] A. J. Leggett, Superfluidity, *Rev. Mod. Phys.* **71**, S318 (1999).
- [26] G. Biagioni, Evidence of superfluidity in a dipolar supersolid, *Il Nuovo Cimento C* **4-5**, <http://dx.doi.org/10.1393/ncc/i2021-21107-5> (2021).
- [27] L. Landau, Theory of the superfluidity of helium ii, *Phys. Rev.* **60**, 356 (1941).
- [28] I. Božović, X. He, J. Wu, and A. T. Bollinger, Dependence of the critical temperature in overdoped copper oxides on superfluid density, *Nature* **536**, 309 (2016).
- [29] L. Tanzi, J. G. Maloberti, G. Biagioni, A. Fioretti, C. Gabbanini, and G. Modugno, Evidence of superfluidity in a dipolar supersolid from nonclassical rotational inertia, *Science* **371**, 1162 (2021).
- [30] M. A. Norcia, E. Poli, C. Politi, L. Klaus, T. Bland, M. J. Mark, L. Santos, R. N. Bisset, and F. Ferlaino, Can angular oscillations probe superfluidity in dipolar supersolids?, *Phys. Rev. Lett.* **129**, 040403 (2022).
- [31] S. M. Rocuzzo, A. Recati, and S. Stringari, Moment of inertia and dynamical rotational response of a supersolid dipolar gas, *Phys. Rev. A* **105**, 023316 (2022).
- [32] P. Ilzhöfer, M. Sohmen, G. Durastante, C. Politi, A. Trautmann, G. Natale, G. Morpurgo, T. Giamarchi, L. Chomaz, M. J. Mark, and F. Ferlaino, Phase coherence in out-of-equilibrium supersolid states of ultracold dipolar atoms, *Nature Physics* **17**, 356 (2021).
- [33] M. E. Fisher, M. N. Barber, and D. Jasnow, Helicity modulus, superfluidity, and scaling in isotropic systems, *Phys. Rev. A* **8**, 1111 (1973).
- [34] A. J. Leggett, On the superfluid fraction of an arbitrary many-body system at $t=0$, *Journal of Statistical Physics* **93**, 927 (1998).
- [35] A. Smerzi, S. Fantoni, S. Giovanazzi, and S. R. Shenoy, Quantum coherent atomic tunneling between two trapped bose-einstein condensates, *Phys. Rev. Lett.* **79**, 4950 (1997).
- [36] I. Zapata, F. Sols, and A. J. Leggett, Josephson effect between trapped bose-einstein condensates, *Phys. Rev. A* **57**, R28 (1998).
- [37] G. Biagioni, N. Antolini, A. Alaña, M. Modugno, A. Fioretti, C. Gabbanini, L. Tanzi, and G. Modugno, Dimensional crossover in the superfluid-supersolid quantum phase transition, *Phys. Rev. X* **12**, 021019 (2022).
- [38] F. S. Cataliotti, S. Burger, C. Fort, P. Maddaloni, F. Minardi, A. Trombettoni, A. Smerzi, and M. Inguscio, Josephson junction arrays with bose-einstein condensates, *Science* **293**, 843 (2001).
- [39] M. Albiez, R. Gati, J. Fölling, S. Hunsmann, M. Cristiani, and M. K. Oberthaler, Direct observation of tunneling and nonlinear self-trapping in a single bosonic josephson junction, *Phys. Rev. Lett.* **95**, 010402 (2005).
- [40] S. Levy, E. Lahoud, I. Shomroni, and J. Steinhauer, The a.c. and d.c. josephson effects in a bose-einstein condensate, *Nature* **449**, 579 (2007).
- [41] G. Valtolina, A. Burchianti, A. Amico, E. Neri, K. Khani, J. A. Seman, A. Trombettoni, A. Smerzi, M. Zaccanti, M. Inguscio, and G. Roati, Josephson effect in fermionic superfluids across the bec-bcs crossover, *Science* **350**, 1505 (2015).
- [42] J. Tao, M. Zhao, and I. B. Spielman, Observation of anisotropic superfluid density in an artificial crystal, *Phys. Rev. Lett.* **131**, 163401 (2023).
- [43] G. Chauveau, C. Maury, F. Rabec, C. Heintze, G. Brochier, S. Nascimbene, J. Dalibard, J. Beugnon,

- S. M. Rocuzzo, and S. Stringari, Superfluid fraction in an interacting spatially modulated bose-einstein condensate, *Phys. Rev. Lett.* **130**, 226003 (2023).
- [44] T. Berrada, S. van Frank, R. Bücke, T. Schumm, J.-F. Schaff, and J. Schmiedmayer, Integrated mach-zehnder interferometer for bose-einstein condensates, *Nature Communications* **4**, 2077 (2013).
- [45] R. Gati, B. Hemmerling, J. Fölling, M. Albiez, and M. K. Oberthaler, Noise thermometry with two weakly coupled bose-einstein condensates, *Phys. Rev. Lett.* **96**, 130404 (2006).
- [46] L. Pezzè, A. Smerzi, M. K. Oberthaler, R. Schmied, and P. Treutlein, Quantum metrology with nonclassical states of atomic ensembles, *Rev. Mod. Phys.* **90**, 035005 (2018).
- [47] E. Lucioni, L. Tanzi, A. Fregosi, J. Catani, S. Gozzini, M. Inguscio, A. Fioretti, C. Gabbanini, and G. Modugno, Dysprosium dipolar bose-einstein condensate with broad feshbach resonances, *Phys. Rev. A* **97**, 060701 (2018).
- [48] F. Böttcher, M. Wenzel, J.-N. Schmidt, M. Guo, T. Langen, I. Ferrier-Barbut, T. Pfau, R. Bombín, J. Sánchez-Baena, J. Boronat, and F. Mazzanti, Dilute dipolar quantum droplets beyond the extended gross-pitaevskii equation, *Phys. Rev. Res.* **1**, 033088 (2019).
- [49] N. Fisher, *Statistical Analysis of Circular Data*, Statistical Analysis of Circular Data (Cambridge University Press, 1995).
- [50] H. Kadau, M. Schmitt, M. Wenzel, C. Wink, T. Maier, I. Ferrier-Barbut, and T. Pfau, Observing the rosenzweig instability of a quantum ferrofluid, *Nature* **530**, 194 (2016).
- [51] A. R. P. Lima and A. Pelster, Quantum fluctuations in dipolar bose gases, *Phys. Rev. A* **84**, 041604 (2011).

Methods

I. SUPERSOLID PREPARATION

The experiment starts from a Bose-Einstein condensate (BEC) of ^{162}Dy atoms trapped in a harmonic potential created by two dipole traps crossing in the horizontal (x,y) plane [47]. To tune the interaction parameter $\epsilon_{dd} = a_{dd}/a_s$, we control the contact scattering length as with magnetic Feshbach resonances, while the dipolar scattering length $a_{dd} = 130 a_0$ is fixed. The condensate is initially prepared at a magnetic field $B \sim 5.5$ G, corresponding to a scattering length of about $140 a_0$. The magnetic field is then slowly changed towards the critical values for the superfluid-supersolid phase transition, close to the set of Feshbach resonances around 5.1 G [7, 48]. We calibrate the magnetic field amplitude via radio-frequency spectroscopy before and after each experimental run. The magnetic field stability is about 0.5 mG, corresponding to a scattering length stability of about $0.25 a_0$. Since the overall systematic uncertainty in the absolute value of a is about $3 a_0$, corresponding to an uncertainty in ϵ_{dd} of about 4%, we identify a precise B -to- a_s conversion by comparing the experimental and numerical data for the critical ϵ_{dd} for the phase transition[37]. The typical atom number in the supersolid is $N = (2.8 \pm 0.3) \times 10^4$. We expect thermal effects to be negligible in the Josephson dynamics, since the coupling energy $K(N_2 + N_3)$ is of the order of $k_B \times 100$ nK in the whole supersolid regime, and from measurements of the thermal fraction on the BEC side we get $T < 30$ nK [7].

II. EXCITATION OF THE JOSEPHSON DYNAMICS

The optical lattice used to excite the Josephson dynamics consists of two repulsive laser beams at 1064 nm that intersect at a small angle, providing a lattice period $d_L = (7.9 \pm 0.3) \mu\text{m}$. The stability of the lattice position is better than 10% of its period over the duration of the experiment (see Fig. S1a), and before each measurement we check the relative position of the lattice and the supersolid. Most of the noise in the excitation protocol comes from shot-to-shot fluctuations of the supersolid lattice due to the Goldstone mode (the position of a single cluster has a standard deviation of the order of 25% of the supersolid period, see below). To calibrate the phase difference imprinted by the optical lattice, we switch on the lattice at fixed $U_{lat} = k_B \times 100$ nK for a variable pulse duration and we measure the imprinted phase difference $\varphi_0 = U_{lat}\tau/\hbar$ immediately after the pulse, see Fig. S1b. In the experiment, we detect clear Josephson oscillations only when the initial imprinted phase is 1 rad or larger. In this regime, we compare the experimental and numerical Josephson frequencies as a function of the amplitude of the oscillation (see Fig. S2). We find a small reduction (about 15%) compared to the small-amplitude regime, which allows us to use the equation $\omega_J^2 = 4KN_3U$ to extract the coupling energy K from the experimental Josephson frequencies. The need for large excitation amplitudes in the experiment can be explained by the presence of the Goldstone mode, which introduces an unavoidable noise on both Z and $\Delta\varphi$. We checked that applying the same phase imprinting protocol to standard Bose-Einstein condensates does not produce any detectable Josephson oscillation, see Fig. S3. This observation can be justified by the fact that the spatially-stationary excitations of the condensate, the rotons, have a spatial period similar to the supersolid period d , so they cannot be excited by the optical lattice with $d_L \sim 2d$. The excitations with spatial period equal to d_L have instead a phonon/maxon character, they are not stationary in the harmonic trap and so they cannot produce spatially stable oscillations. In general, this observation proves that the self-induced

Josephson oscillations exist in the supersolid but not in the superfluid. We cannot make reliable experiments in the solid-like droplet-crystal phase, due to the exceedingly short lifetime of the experimental system in that regime, but the simulations show that the Josephson coupling becomes negligible and Josephson oscillations are absent.

III. PHASE DETECTION AND ANALYSIS

To measure the phase difference between the two central clusters of the supersolid, $\Delta\varphi = \varphi_3 - \varphi_4$, we record the atomic distribution in the (x,y) plane by absorption imaging after 61 ms of free expansion. About 200 μs before releasing the atoms from the trapping potential, we increase the contact interaction strength by setting $a_s = 140 a_0$, thus minimising the relative effects of the long-range dipolar interaction on the expansion. We interpret the recorded distributions as the atomic density in momentum space, $\rho(k_x, k_y)$. In the supersolid regime, the momentum distribution shows an interference pattern due to the superposition of the expanding matter-waves of each cluster (see snapshots in Fig. 2a). We first integrate the two-dimensional distribution over k_y to obtain the one-dimensional momentum distribution $\rho(k_x)$. We then fit $\rho(k_x)$ with a double-slit model:

$$\rho(k_x) = G(k_x, k_0, \sigma) \left[1 + A_1 \cos^2 \left(\pi(k_x - k_0)/k_r + \theta \right) \right] \quad (\text{S1})$$

where $G(k_x, k_0, \sigma)$, is a gaussian envelope of centre k_0 and width σ , while A_1, k_r and θ are the amplitude, period and phase of the modulation, respectively. Due to the $\cos^2(x)$ term in our fit function, the physical phase difference is given by $\Delta\varphi = 2\theta$. Although the interference pattern is generated by six overlapping clusters, $\Delta\varphi$ can be extracted with a good approximation (within 20%) by the double-slit model due to the finite resolution of our imaging system in momentum space ($0.2 \mu\text{m}^{-1}$, 1/e Gaussian width) and to the lower weight of lateral clusters. This is experimentally confirmed by the measured imprinted phase φ_0 as a function of the pulse depth, shown in Fig. S1, which is in good agreement with the prediction for the phase difference between adjacent clusters, $U_{lat}\tau/\hbar$. For each observation time t , we take $n = 20 - 30$ images. We then calculate the mean value of $\Delta\varphi$ using the circular mean, which is appropriate for a periodic quantity such as an angle:

$$\overline{\Delta\varphi} = \arg \left(\sum_{j=1}^n e^{i\Delta\varphi_j} \right) \quad (\text{S2})$$

where $\arg(x)$ indicates the argument of the complex number x and i is the imaginary unit. The corresponding error is given by the circular standard deviation[49].

IV. IMBALANCE DETECTION AND ANALYSIS

To measure the population imbalance between clusters, we image the supersolid in-situ in the (x,y) plane using an imaging system with a resolution of 2.5 μm , smaller than the cluster spacing of 4 μm . To avoid saturation effects due to the high density of the sample, we use dispersive phase-contrast imaging [50] with an optical beam detuned by 5 Γ from the 421 nm optical transition. From each experimental shot, we calculate the imbalance as follows. We integrate the column density along the y -direction (transverse to the modulation) obtaining 1D density profiles where we identify the two main peaks (snapshots in Fig. 2b). We then measure the populations $N_1 + N_2 + N_3$ and $N_4 + N_5 + N_6$ integrating the signal to the left and to the right of the minimum between the clusters, respectively. We then compute the observable $Z = (N_6 + N_5 + N_4 - N_3 - N_2 - N_1)/N$.

Due to the limited optical resolution, we can clearly resolve the left and right clusters populations only when the contrast of the density modulation is high enough, i.e. only at $\epsilon_{dd} = 1.444$. For lower ϵ_{dd} , we use an optical separation technique to increase the signal-to-noise ratio. We turn on the optical lattice used for the excitation 5 ms before image acquisition. This causes the main clusters to move away, falling into the minima of the optical potential and increasing their distance (snapshots in Fig. 2a and in Fig. S4). Although our lattice does not have the optimal spatial phase to separate the clusters, since it has a maximum at the position of one cluster, we checked with numerical simulations that the only effect on the imbalance Z is the addition of a constant offset, thus not changing the oscillation frequency (see Fig. S4). Experimentally, we checked that the Josephson frequencies measured with and without the optical separation, are consistent within one standard deviation (see filled and empty blue points at $\epsilon_{dd} = 1.444$ in Fig. 4). At lower ϵ_{dd} , very close to the phase transition, the contrast is too low, so we rely only on phase measurements.

V. EXPERIMENTAL MEASUREMENT OF THE SUPERFLUID FRACTION FROM THE JOSEPHSON FREQUENCY

To measure the superfluid fraction in the whole supersolid regime, reported in Fig. 4, we employ the Josephson frequency ω_J extracted from phase oscillations. We use the formula $f_s = \frac{\omega_J^2/(4N_{34}U)}{\hbar^2/(2md^2)}$. The period d of the supersolid lattice is measured with in situ imaging, obtaining $d = 3.7 \pm 0.1 \mu\text{m}$. The quantity $N_{34}U$ is taken from the numerical simulations. Since the experimental oscillations are not in the small amplitude limit, the frequencies are underestimated by about 15% (see Fig. S2). The upper error bar for f_s in Fig. 4 includes accordingly a 15% uncertainty. For the experimental configurations where we measure both Z and $\Delta\varphi$, we also checked that U extracted from Eq. 4b is in agreement with the simulations.

VI. DISCUSSION OF THE LEGGETT MODEL

Leggett derived the upper bound for the superfluid fraction f_s^u in the case of a 1D system rotating in an annulus with radius R , for which the moment of inertia is $I = (1 - f_s)I_c$, with I_c the classical moment of inertia [16]. To find the phase profile $\varphi(x)$ that minimises the kinetic energy for a fixed number density $n(x)$, one has to work in the frame corotating with the annulus, in which the external potential is time-independent. In this frame, the rotation imposes a phase twist between neighbouring clusters, proportional to the angular velocity Ω of the annulus, $\Delta\varphi = \varphi(d) - \varphi(0) = m\Omega R d/\hbar$. The result of the energy minimisation is $\varphi(x) = \int_0^x dx' n(x')^{-1} / \int_0^d dx' n(x')^{-1}$ and the corresponding kinetic energy cost is $E_{kin}(\Delta\varphi) = N\hbar^2/(2md^2)f_s^u\Delta\varphi^2$, where f_s^u is the upper bound of Eq. 2. The lower bound f_s^l , instead, is found starting from the 3D kinetic energy, which includes also the derivatives along the transverse directions y and z [34]. It reads $f_s^l = \int dydz \left(1/d \int_0^d dx/\bar{n}(x,y,z)\right)^{-1}$, where $\bar{n}(x,y,z)$ is the normalised 3D density. From the expression of the energy, we see that the superfluid fraction has the role of an elastic constant for the phase deformation. The density and phase profiles sketched in Fig. 1b, and the corresponding energy density $\hbar^2/(2m)n(x)|\nabla\varphi(x)|^2$, are for an hypothetical homogeneous supersolid lattice with $f_s = 0.20$. In the Josephson case, the phase twist is externally applied with an odd parity, to induce Josephson oscillations between neighbouring sites. The energy minimisation on the single cell gives the same result as before, since it is insensitive to the sign of the phase twist. In the sketch of Fig. 1c we build the odd phase profile by changing sign from cell to cell to $\varphi(x)$ of Fig. 1b.

VII. GOLDSTONE MODE

In a harmonic trap, the Goldstone mode energy $\hbar\omega_G$ is finite but much smaller than $\hbar\omega_x$, since the supersolid can rearrange its density to minimise the centre of mass displacement. The resulting dynamics is an oscillation of the lattice position, imbalance and relative phase. Due to its low frequency, the Goldstone mode is thermally activated. Similarly to previous works [24], we detect the Goldstone excitation as fluctuations in the lattice position that keep the centre of mass fixed (see Fig. S5). We prepare the supersolid with three main clusters and, without any additional manipulation, we probe the in-situ density. We detect fluctuations in the cluster positions, with standard deviation $\sigma_{\text{clusters}} \sim 1 \mu\text{m}$, much larger than the centre of mass fluctuations, $\sigma_{\text{com}} \sim 0.4 \mu\text{m}$. The Goldstone mode also introduces some noise in Z and $\Delta\varphi$ during the dynamics, which we estimate to be about 20% of the Josephson amplitude, for both observables.

The frequency of the Goldstone mode can be observed in numerical simulations at $T = 0$ by setting an initial $Z_0 > 0$ together with a small displacement of the weak link position, $x_0 \neq 0$, see Fig. S5. In the time evolution of Z , we find a very low frequency oscillation, $\omega_G = 2\pi \times (3.56 \pm 0.08)$ Hz, on top of the Josephson dynamics, $\omega_J = 2\pi \times (23.85 \pm 0.03)$ Hz. We find similar values for $\Delta\varphi$. The weak link position oscillates at the same low frequency ω_G .

VIII. NUMERICAL SIMULATIONS

To simulate the dynamics of our system we numerically integrate the extended Gross-Pitaevskii equation (eGPE):

$$i\hbar \frac{\partial}{\partial t} \psi(\mathbf{r}, t) = \left[-\frac{\hbar^2}{2m} \nabla^2 + V_{h.o.}(\mathbf{r}) + g|\psi(\mathbf{r}, t)|^2 + V_{dd}(|\mathbf{r} - \mathbf{r}'|) + \gamma(\epsilon_{dd})|\psi(\mathbf{r}, t)|^3 \right] \psi(\mathbf{r}, t). \quad (\text{S3})$$

where $V_{h.o.}(\mathbf{r}) = 1/2m(\omega_x^2 x^2 + \omega_y^2 y^2 + \omega_z^2 z^2)$ is the harmonic external potential, $g = 4\pi\hbar^2 a_s/m$ is the contact interaction parameter, $V_{dd}(\mathbf{r}) = \frac{C_{dd}}{4\pi} \frac{1-3\cos^2\theta}{r^3}$ is the dipolar interaction, with θ the angle between \mathbf{r} and z and $C_{dd} = 3\epsilon_{dd}g$. The last term is the Lee-Huang-Yang energy of quantum fluctuations [51]. Josephson dynamics was induced either by an antisymmetric phase imbalance imprinted with a sinusoidal potential as in the experiment, or by an initial antisymmetric population imbalance. Both methods excite the same Josephson normal mode. Atom number and phase for each cluster are calculated at each time step by determining the position of the density minima between the clusters, eliminating their slow and weak oscillations. The superfluid fraction in Fig. 4a (green dots) is obtained by calculating the coupling energy K in the limit of small initial imbalance ($Z(0) \sim 0.01$), finding values in the range $K = k_B \times (0.1 - 0.01)$ nK. From Eq. 4b we find $N_{34}U = k_B \times (5 - 7)$ nK, slowly varying with ϵ_{dd} . The ratio $N_{34}U/(2K)$ is always larger than 25.

IX. SIX-MODE JOSEPHSON MODEL

We employ a set of six-mode Josephson equations with interaction parameters U_j , with $j = 1, \dots, 6$ labelling the clusters, five coupling parameters between adjacent clusters $K_{j,j+1}$, and energy offsets E_0 and E_1 , for the opposite side clusters 1 and 6, and 2 and 5, due to the harmonic trap. We indicate as $K = K_{34}$ and $U = U_3 = U_4$ the coupling and interaction energy, respectively, in two central clusters. The symmetry of the system further allows us to equalise the two side coupling $K' = K_{23} = K_{45}$ and $K'' = K_{12} = K_{56}$, the two side interactions $U' = U_2 = U_5$ and $U'' = U_1 = U_6$ (see Fig. 2a). We thus have a system of six equations for the time evolution of the populations N_j and five phase differences $\varphi_{ij} = \varphi_i - \varphi_j$:

$$\begin{aligned}\dot{N}_1 &= -2K''\sqrt{N_2N_1}\sin\varphi_{21}, \\ \dot{N}_2 &= 2K''\sqrt{N_2N_1}\sin\varphi_{21} - 2K'\sqrt{N_3N_2}\sin\varphi_{32}, \\ \dot{N}_3 &= 2K'\sqrt{N_3N_2}\sin\varphi_{32} - 2K\sqrt{N_4N_3}\sin\varphi_{43}, \\ \dot{N}_4 &= 2K\sqrt{N_4N_3}\sin\varphi_{43} - 2K'\sqrt{N_5N_4}\sin\varphi_{54}, \\ \dot{N}_5 &= 2K'\sqrt{N_5N_4}\sin\varphi_{54} - 2K''\sqrt{N_6N_5}\sin\varphi_{65}, \\ \dot{N}_6 &= 2K''\sqrt{N_6N_5}\sin\varphi_{65},\end{aligned}\tag{S4a}$$

$$\begin{aligned}\dot{\varphi}_{21} &= E_1 + U''N_1 - U'N_2, \\ \dot{\varphi}_{32} &= E_0 + U'N_2 - UN_3, \\ \dot{\varphi}_{43} &= U(N_3 - N_4), \\ \dot{\varphi}_{54} &= -E_0 + UN_4 - U'N_5, \\ \dot{\varphi}_{65} &= -E_1 + U'N_5 - U''N_6,\end{aligned}\tag{S4b}$$

where we have considered the case $(N_4 + N_3)U/(2K) \gg 1$ so that we have neglected the tunnelling terms in the evolution of the phases.

In the following we further consider small amplitude oscillations such that we can replace $\sqrt{N_iN_j} \sim \sqrt{N_i(0)N_j(0)}$ and $\sin\varphi_{ij} \sim \varphi_{ij}$ into Eq. S4a, where $N_j(0)$ is the initial population of the j th cluster at time $t = 0$. For symmetry reasons, we have $N_1(0) \sim N_6(0)$, $N_2(0) \sim N_5(0)$, and $N_3(0) \sim N_4(0)$. Even in the linear regime, the time evolution of populations and phases predicted by Eqs. S4 shows multiple frequencies. Harmonic single-frequency oscillations with a $\pi/2$ phase shift between populations and relative phases are observed under the two conditions

$$\begin{aligned}\frac{U''}{U'} &= 1 + \frac{K'}{K''}\sqrt{\frac{N_3(0)}{N_1(0)}}, \\ \frac{U'}{U} &= \frac{1 + \frac{K}{K'}\sqrt{\frac{N_3(0)}{N_2(0)}}}{1 + \frac{K''}{K'}\sqrt{\frac{N_1(0)}{N_3(0)}}}.\end{aligned}\tag{S5}$$

In particular, under these conditions, we have

$$\dot{N}_3 - \dot{N}_4 = \alpha(\dot{N}_6 - \dot{N}_1 + \dot{N}_5 - \dot{N}_2),\tag{S6}$$

where $\alpha = 1/(U/U' - U/U'')$. The corresponding Josephson oscillation frequency is

$$\omega_J^2 = 2KU[N_3(0) + N_4(0)] \frac{\alpha}{\alpha - 1}. \quad (\text{S7})$$

To evaluate the parameters in the above equations and verify Eq. S5, we insert into Eqs. S4 the numerical results for $N_j(t)$ and $\varphi_{ij}(t)$ obtained from GPE simulations. A comparison between GPEs oscillations and the six-mode model is shown in Fig. S6. First, the GPE ground state gives $N_3(0) = N_4(0) \sim N/4$, while the population of the lateral clusters depends on ϵ_{dd} . In particular, outer clusters $N_1(0) = N_6(0)$ decrease, while $N_2(0) = N_5(0)$ increase as ϵ_{dd} increases. The parameters U and K of the central clusters are extracted from Eqs. 4 in the main text. The other parameters U', U'', K' and K'' are extracted from fits using Eqs. S4. Overall, we obtain that the interactions parameters are $U/U' \sim 1$, $U/U'' \sim 1/2$ within fluctuations of about 10% for different values of ϵ_{dd} . On the other hand, the coupling ratio $K/K' \sim 0.6$ is constant, while $K/K'' \sim 0.7$ on the BEC side and decreases with ϵ_{dd} , as do the initial external populations $N_1(0) = N_6(0)$. We thus find that Eq. S6 is fulfilled and $\alpha = 2$. For this value of α , Eq. S7 gives $\omega_J^2 = 4KU[N_3(0) + N_4(0)]$, in agreement with the main text.

Taking into account Eq. S6 and the symmetry condition $N_3(0) = N_4(0)$, we find $N_3 - N_4 = (N_6 - N_1 + N_5 - N_2)$ at each time. We thus have $Z = (\alpha - 1)/\alpha \Delta N/N$, with $\Delta N = N_3 - N_4$. This reduces to $\Delta N = 2NZ$ for $\alpha = 2$. Using Eq. 4a, we have $\dot{Z} = -4K \sqrt{N_4(0)N_3(0)}/N \sin \Delta\varphi$, with $\Delta\varphi = \varphi_{43}$. We can write $2\sqrt{N_3(0)N_4(0)} = N_3(0) + N_4(0) = N_{34}$ and get $\dot{Z} = -2KN_{34}/N \sin \Delta\varphi$. The evolution of the phase difference $\Delta\varphi = U(N_3 - N_4)$, see Eq. S4b, rewrites as $\dot{\Delta\varphi} = U\Delta N = 2NUZ$.

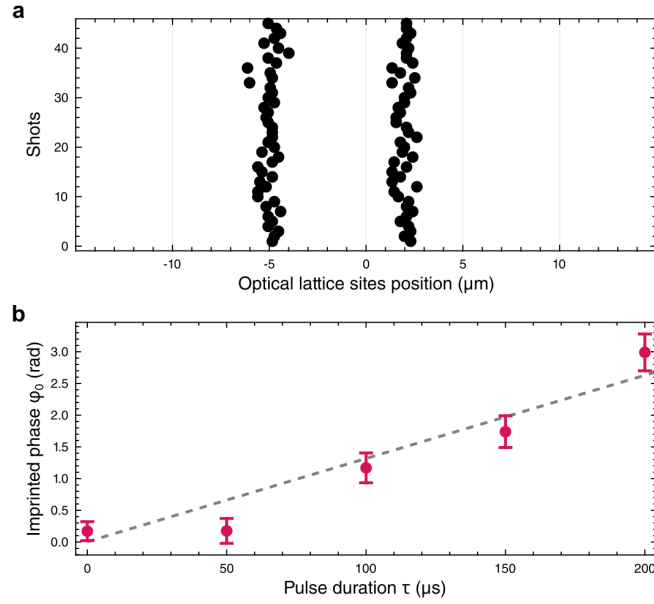


FIG. S1. (a) Stability of the optical lattice. Black dots are the relative positions of the density peaks of a BEC loaded into the optical lattice with respect to the average centre of mass, for 45 different shots. The standard deviation of fluctuations for each lattice position is $\sigma_{lattice}$ 0.35 μm . (b) Calibration of the initial phase difference imprinted on the two main clusters as a function of the lattice pulse duration. Red dots are experimental data obtained by imprinting the optical lattice potential for different pulse durations. The dashed line is the theoretical prediction $U_{lat}\tau/\hbar$ with a lattice depth $U_{lat} = k_B \times 100$ nK.

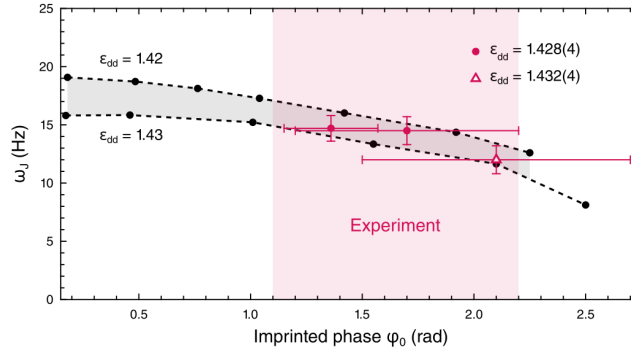


FIG. S2. Josephson frequency as a function of the phase amplitude, theory (black points) and experiment (red points). For typical experimental amplitudes $\pi/2$, we observe a frequency reduction of about 15% compared to the small excitation regime. The highlighted region is the relevant one for our experiment.

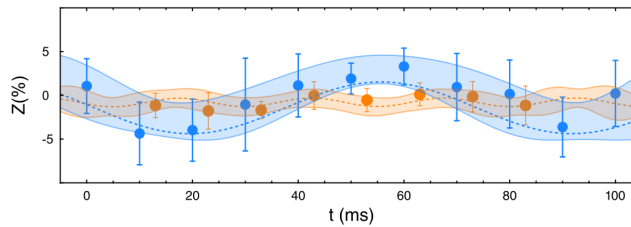


FIG. S3. Absence of Josephson oscillations for a standard Bose-Einstein condensate. Time evolution of the population imbalance after the phase imprinting for a supersolid (blue) and an unmodulated BEC (orange), extracted using the optical separation. The dashed lines are sinusoidal fits with confidence bands (for 1σ) in shaded colour. The fitted oscillation amplitude of the BEC is compatible with zero.

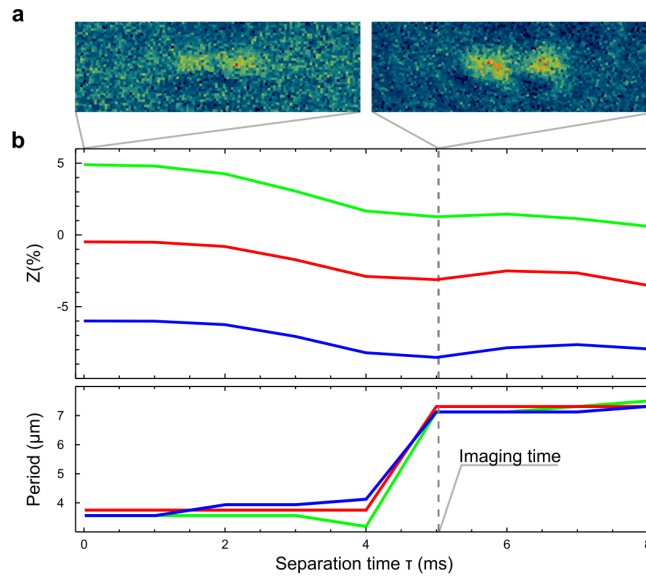


FIG. S4. Analysis of the optical separation technique. (a) Experimental in-situ images of two balanced ($Z = 0$) supersolids without any manipulation (left) and using the optical separation (right). (b) Numerical simulation of the dynamics of three different supersolids with initial population imbalance $Z_0 = 5\%$ (green), $Z_0 = 0\%$ (red) and $Z_0 = -5\%$ (blue), during the optical separation. Top row: imbalance Z . Bottom row: distance between the central clusters.

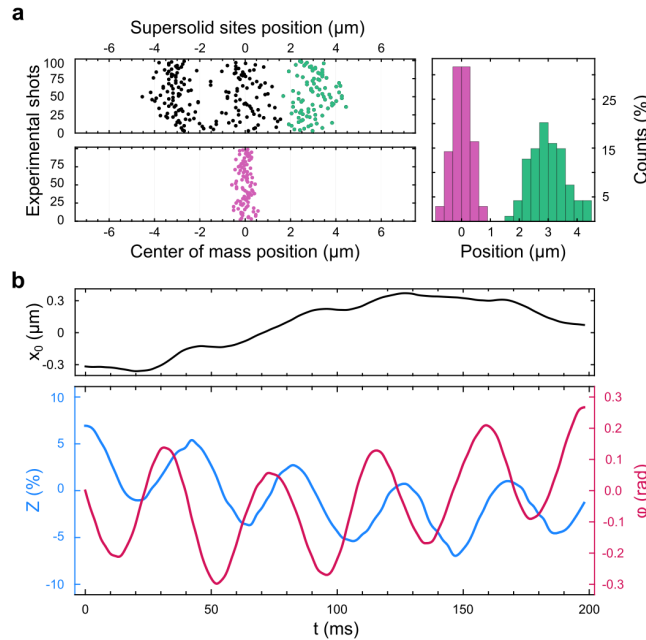


FIG. S5. Evidence of the Goldstone mode in experimental and numerical data. (a) Left panels: fluctuations of the clusters positions (black and green points) and centre of mass (pink points) of the supersolid for about 100 experimental shots. Right panel: histograms of the right-cluster (green) and of the centre of mass (pink) positions. (b) Simulation of the Josephson dynamics coupled to the Goldstone oscillation. The position of the density minimum x_0 (top row) shows a clear oscillation at the Goldstone frequency $\omega_G \ll \omega_J$. This lower frequency appears also in Z and (bottom row) on top of the standard Josephson dynamics.

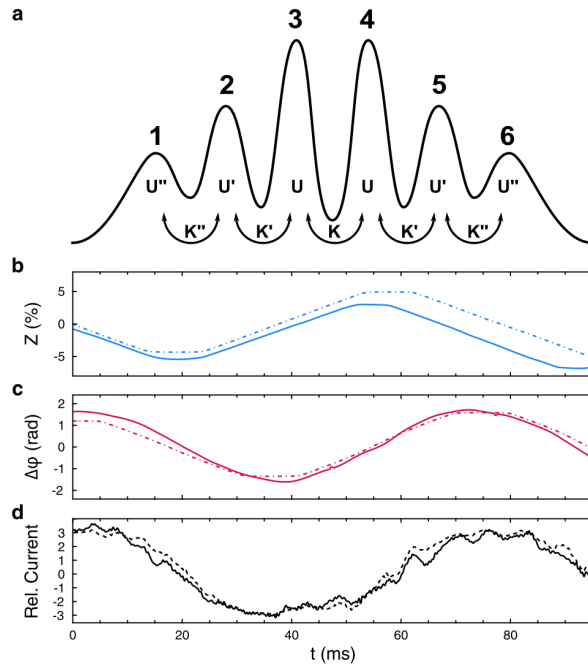


FIG. S6. Six-mode model and numerical simulations. (a) Sketch of the inhomogeneous system with six clusters with interaction energies U , U' and U'' , with coupling energies K , K' and K'' . The modes in the sketch are not on scale (compare with the simulation of our system in Fig. 2a in the main text). (b-c) Comparison between the time evolution calculated from the GPE simulations (thick lines) and from the six-mode model (dot-dashed lines) for Z (b) and (c). (d) Relative currents between the central and lateral clusters appearing in Eq. S6, from GPE simulations. The solid line is $(N_3 - N_4)/2$ while the dashed line is $(N_6 + N_5 - N_2 - N_1)$.